Biomanufacturing of Value-Added Products from Oils or Fats: A Case Study of *Yarrowia lipolytica*

Na Liu, Ya-Hue Valerie Soong, Iman Mirzaee, Andrew Olsen, Peng Yu, His-Wu Wong, Dongming Xie*

[a] Department of Chemical Engineering, University of Massachusetts Lowell, One University Avenue, Lowell, MA 01854, USA.

*Corresponding authors: Dongming Xie (Tel: +1-978-934-3159; Email: Dongming_Xie@uml.edu).

Abstract

The United States produces more than 10 million tons of waste oils and fats each year. This paper aims to establish a new biomanufacturing platform that convert waste oils or fats into a series of value-added products. Our research employs the oleaginous yeast *Yarrowia lipolytica* as a case study for citrate production from waste oils. First, we conducted the CFD simulation of the bioreactor system and identified that the extracellular mixing and mass transfer is the first limiting factor of an oil fermentation process due to the insolubility of oil in water. Based on the CFD simulation results, bioreactor design and operating conditions were optimized and successfully enhanced oil uptake and bioconversion in fed-batch fermentation experiments. After that, we investigated the impacts of cell morphology on oil uptake, intracellular lipid accumulation, and citrate formation by overexpressing and deleting the *MHY1* gene in the wild type *Y. lipolytica*. Fairly good correlations were achieved between cell morphology and productivities of biomass, lipid, and citrate. Finally, fermentation kinetics with both glucose and oil substrates were compared and the oil fermentation process was carefully evaluated. Our research results suggest that waste oils or fats can be economical feedstocks for biomanufacturing of many high-value products.

Keywords: *Y. lipolytica,* biomanufacturing, waste oils, CFD simulation, cell morphology

Notation

μ_{max}	maximum specific growth rate (h^{-1})
L	total intracellular lipid (g/L)
S	carbon source substrate (glucose, SbO or WCO) (g/L)
SbO	soybean oil
WCO	waste cooking oil (canola seed oil after French frying process)
$Y_{X/S}$	biomass yield (g formed biomass per g of substrate consumed)
$Y_{CA/S}$	citric acid yield (g formed CA per g of substrate consumed)
$Y_{L/S}$	lipid yield (g formed lipid per g of substrate consumed)

Introduction

The oleaginous yeast *Yarrowia lipolytica* is one of the most extensively studied "non-conventional" yeasts. Due to its prominent ability to utilize hydrophobic carbon sources, such as oils and fats, and outstanding capability of producing various important intracellular and extracellular metabolites as valuable products, *Y. lipolytica* has attracted more and more attention as a superior host for metabolic engineering. The distinct propensity for high flux through tricarboxylic acid (TCA) cycle intermediates and biological precursors such as acetyl-CoA and malonyl-CoA has highlighted *Y. lipolytica* as a cell factory with a unique potential for a variety of biomanufacturing products. With the recent developments in synthetic biology tools, the industrial potential of *Y. lipolytica* has been expanded to numerous products, including organic acids (e. g., citric acid, α-ketoglutaric acid, and itaconic acid) (Abghari & Chen, 2017; Zeng et al., 2017; Zhou et al., 2010), proteins (e.g., lipases, RNase, and esterase) (Fickers et al., 2005a; Soong et al., 2019), lipids and lipid-derived products (e.g., biodiesel, single-cell oil, and omega-3) (Mlickova et al., 2004; Xue et al., 2013, Zhu & Jackson, 2015).

Most of biomanufacturing processes use sugars such as glucose as the carbon and energy source, which are derived from the agriculture crops or residues including corn starch, corn stover, or other types of cellulosic biomass. However, using the starch-based sugar for biomanufacturing leads to a concern of competition with food production; the fluctuations in glucose market also brings in uncertainties in supply chain and the profitability (Liu et al. 2020). At the same time, the United States produces about 20 million tons of vegetable oils every year, which is about the twice as much as the total sugar production (Liu et al. 2020). Plant oils are mainly used for food and feed application and generates low or limited economical values. A significant portion of oils/fats is wasted after the primary applications. Even though some of WCO is used for the production of biodiesel (Du et al. 2008, Refaat 2010) or other chemical products, a significant portion is discharged into the environment and causes pollution concerns. If WCO can be used as the raw material for biomanufacturing of value-added products, this

would help avoid or minimize the pollution issue as well as improve the economical values of original or wasted oils and fats.

The yeast *Y. lipolytica* is able to directly grow on plant oils or animal fats and further convert them into many bio-privileged molecules, which provides us a new economical choice of raw materials for biomanufacturing. *Y. lipolytica* is often found in habitats containing lipids, such as dairy products, oil polluted environments and raw poultry (Coelho et al. 2010), and has developed sophisticated mechanisms for efficient use of lipids. The common format of plant oils and animal fats is triacylglycerol (TAG), which is formed by esterification of glycerol with three free fatty acids (FFAs). In order to directly metabolize TAG-based oils and fats, *Y. lipolytica* must first degrade TAG to FFAs and glycerol in the fermentation medium with the catalysis of lipase as no known TAG transporters have been identified (Beopoulos et al. 2009). Subsequently, the extracellular FFAs are imported inside the cells for further utilization by either transporters or diffusion at concentrations above 10 μM (Kohlwein & Paltauf 1983). Once in the cytoplasm, FFAs could be activated by cytoplasmic acyl-CoA synthase FAA1 to form fatty acyl-CoA. Fatty acyl-CoA can then be either stored in lipid bodies (LB) as TAG or be transported directly into peroxisomes and be degraded as a result of the well-studied β-oxidation (Fig. 1).

Once an oil/fat substrate is chosen as the main carbon and energy source for large scale of biomanufacturing, efficient extracellular lipid-water mixing and mass transfer need to be achieved in the bioreactor environment. However, one major challenge for the fermentation with lipid substrates is the poor mixing and mass transfer of lipids in a bioreactor environment due to the insolubility of lipids in aqueous medium (Lucatero et al., 2003). Although *Y. lipolytica* can produce some surfactants to help emulsify lipids in aqueous phase, the overall mixing efficiency still largely depends on the bioreactor design (e.g., impeller design) and operation conditions (e.g., power input of agitation) (Menisher et al., 2000; Xie et al., 2017). Computational fluid dynamics (CFD) is an invaluable tool that could be applied to understand and analyze the mixing of multi-phase flows in a bioreactor, which enables a better understanding of the role of

the hydrodynamic environment and provides guidance for further optimization of the bioreactor design and operating conditions.

It is also believed that cell morphology has a strong influence on interactions between extracellular substrate and individual cells and the mixing and mass transfer in a multi-phase biotechnological process (Driouch et al., 2010; Zhang et al., 2007). As a dimorphic yeast, *Y. lipolytica* is capable of alternation between a unicellular yeast form and distinct filamentous shapes (pseudohypha and hypha) (Bankar et al., 2018; Morales-Vargas et al., 2012). The yeast-to-hypha transition could be induced in stressful environment with nutrient limitation, high osmotic pressure, or anaerobic stress (Domínguez et al., 2000; Kawasse et al., 2003; Ruiz-Herrera & Sentandreu, 2002). It could also be regulated by genes such as *MHY1, BEM1,*and *RAS2* (Cervantes-Chavez & Ruiz-Herrera, 2007; Hurtado & Rachubinski, 1999; Lee & Kronstad, 2002). Among these genes, *MHY1* encoding a C_2H_2-type zinc finger protein, MHY1p, which promotes the yeast-to-hypha transition of *Y. lipolytica*; disruption of the *MHY1* prevents hypha formation (Wang et al., 2018).

In this study, we used the oleaginous yeast *Y. lipolytica* as a model organism to study the critical factors that impact the biomanufacturing of value-added products from various plant oil substrates, including SbO and WCO. CFD simulation was used to understand hydrodynamic characteristics of stirred tank bioreactors with oil-water mixing. The results were further used to optimize the impeller design and the agitation speed of the bioreactor during real fermentation experiments. To examine the effect of cell morphology on the fermentation with lipid substrates, the hyphal strain VSYM1 and the yeast-like strain VSYM2 were generated by overexpression and disruption of the gene *MHY1*, respectively, in the wild type *Y. lipolytica* ATCC20362. Fermentation kinetics of cell growth, lipid accumulation, and citric acid (CA) production from glucose, SbO, and WCO were evaluated and compared for cells with different morphologies.

Materials and methods

Strains

The yeast strains used in this study included the wild type *Y. lipolytica* ATCC20362 and its derivatives (Table 1). The uracil auxotrophic variant of ATCC20362, VSYU1, was used as the parent strain for VSYM1 and VSYM2. The hyphal strain VSYM1 was generated from VSYU1 by overexpression of *MHY1* and fixing the *URA3* in VSYU1. The yeast-like strain VSYM2 was generated by deletion of *MHY1* and fixing *URA3* in VSYU1. *E. coli* strain NEB5α (New England Biolabs, NEB) was used for cloning and plasmid propagation. NEB5α was grown at 37℃ with constant shaking in lysogeny broth medium supplemented with 100 mg/ml of ampicillin for plasmid propagation.

Plasmid and strain construction

Cloning procedures:

All primers used in the study are listed in the Supplementary Table S1. Plasmids were constructed by connecting DNA fragments with HiFi DNA assembly (NEBuilder HiFi DNA Assembly Cloning Kit, NEB) according to the manufacturer's protocol. All restriction enzymes were purchased from NEB and all digestions were performed according to standard protocols. Genomic DNA was extracted from *Y. lipolytica* using the Wizard Genomic DNA Purification kit (Promega). Desired genes were amplified by PCR reactions, which were set up with recommended conditions using Q5 high-fidelity DNA polymerase (NEB) or Taq DNA polymerase (NEB). Gel extractions were performed using the QiAquick Gel Extraction kit. All plasmids were first assembled in *E. coli* strain NEB5α and then extracted by using ZymoPURE Plasmid Miniprep Kit (Zymo Research Corporation).

Construction and transformation of pMHY1 plasmid

The DNA sequence corresponding to the *MHY1* and *URA3* were amplified from ATCC20362

genomic DNA, and the *MHY1* gene expression was under the control of pTEF1 promoter amplified from the ATCC20362 genomic DNA and CYC1 terminator amplified from the *Saccharomyces cerevisiae* S288C genomic DNA. Four DNA fragments were then cloned into the pUC19 by HiFi assembly. The *MHY1* overexpression cassette (4,362bp) was linearized from pMHY1 plasmid by SphI/SspI restriction enzyme digestion. Transformation of the yeast cells with linear gene cassette was carried out using the Frozen-EZ Yeast Transformation II™ kit (Zymo Research) according to manufacturer's instructions. The VSYM1 strain was generated by random insertion of linear *MHY1* overexpression cassette into VSYU1 genome.

Construction and transformation of pMHY1KO plasmid

The DNA sequence corresponding to the *URA3* amplified from ATCC20362 genomic DNA was flanked by the 500 bp *MHY1* promoter and terminator as left and right homologous arms. Three DNA fragments were then cloned into the pUC19 by HiFi assembly. The linearized *MHY1* knockout cassette (2,956bp) was obtained by PCR using the plasmid pMHY1KO as template with primers 5'MHY1-HR-sFP and U3'MHY1-HR-sRP. The VSYM2 was generated by integration of linear *MHY1* knockout cassette into VSYU1 chromosome via homologous recombination.

Shake flask culture protocol

Shake flask culture was prepared by transferring 0.5 mL cells from seed vial to a 250-mL flask containing 50 mL of nitrogen-limited medium, which consisted of Bacto™ yeast extract (2.5 g/L), $(NH_4)_2SO_4$ (1 g/L), KH_2PO_4 (6 g/L), and K_2HPO_4 (2 g/L), 1 M $MgSO_4$ (1 mL/L), 100x trace metals stock solution (Xie at al., 2017) (0.5 mL/L), and supplemented with different sole carbon source: glucose (40 g/L), SbO (Sigma-Aldrich) (25 mL/L) or WCO (french-fried canola oil obtained from a local restaurant) (25 mL/L). The composition of fatty acids in SbO and WCO were analyzed using gas chromatography coupled to a flame ionization detector (GC-FID)

(Table 2). Glucose feed solution (600 g/L) was fed in two shots at 48 h (2 mL) and 96 h (2 mL), respectively. SbO or WCO were fed in at 48 h (0.6 mL) and 96 h (0.6 mL), respectively. One milliliter of phosphate buffer (6 g/L KH_2PO_4, and 2 g/L K_2HPO_4, 14 g/L $NaHCO_3$) was added to the culture media every 24 h for the pH adjustment. The flask culture cells were grown in flask for 6 days at 30℃, 280 rpm in a New Brunswick G25 Shaker Incubator. All flask culture experiments were performed in duplicate.

Fed-batch fermentation protocols

Seed cells were grown at 30℃, 250 rpm for 18~24 h in 250-ml flasks containing 50 mL culture medium, which consisted of Bacto™ yeast extract (5.0 g/L), $(NH_4)_2SO_4$ (5.0 g/L), KH_2PO_4 (6.0 g/L), Na_2HPO_4 (2.0 g/L), and glucose (20.0 g/L). When the OD600 of seed culture reached 2~4, the whole flask of culture was transferred to a 1-L bioreactor (Sartorius B-DCU, Germany) containing 0.7 L fermentation medium, as described by Xie et al. (2017). The initial fermentation medium contained 50 g/L glucose or 40 mL/L SbO or WCO as the sole carbon source. The pO_2 level of the fermentation was set at 30% of air saturation by cascade controls of agitation speed between 500 and 1,400 rpm unless otherwise specified and pure oxygen enrichment (if needed). The aeration rate was fixed at 0.3 L/min and the temperature was maintained at 30℃ throughout the run. The pH was controlled at 6.0 during 0~12 h and then increased to 7.0 in 6 hours and maintained at 7.0 in the remainder of the run by feeding KOH (56% w/v). Glucose (600 g/L), SbO or WCO feeding commenced at around 14 h. The residual substrates were maintained at 20~30 g/L by adjusting feed rate based on off-line measurements. Experiments were performed in duplicate.

Analytical methods

Determination of dry cells weight, residual substrates, citric acid, and lipid bodies

To measure dry cells weight (DCW), cells from 5 mL of culture broth were harvested by

centrifugation at 4,300 g for five minutes and washed three times with distilled water. The cells were dried at 95℃ for 12~24 h until a constant weight reached. The residual glucose in fermentation media was measured with the Stanbio enzymic glucose assay kit (VWR, USA). The residual oils and FFAs were estimated based on a simple spectrophotometric method for the determination of fatty acids (FAs) using triethanolamine–copper salts method (Chen & Vaidyanathan, 2012). The concentration of CA was measured with the EnzyChrom™ Citrate Assay Kit (VWR, USA). The intracellular lipid bodies (LBs) were stained with Sudan black B (SBB) according to the procedure described previously by Du et al. (2014). The stained LBs were observed using a light microscope (Motic), equipped with a microscope camera.

Qualitative and quantitative analysis of intracellular lipids

Lipids synthesized by *Y. lipolytica* were quantified using GC-FID, the lipids (mainly TAGs and FFAs) were converted into their fatty acid methyl esters (FAMEs). The resulting FAMEs were analyzed by a Shimadzu GC2010 Plus GC with an FID according to the procedure modified from a previously described procedure (Xu et al., 2017). Detailed information about the procedure is shown in supplementary.

Analysis of cell morphology

The morphology of *Y. lipolytica* cells was observed under a light microscope (Motic) and analyzed by the software MoticImages Plus 3.0. At least 100 cells were analyzed for each sample. Two parameters, the Elongation (E) and Morphology number (MN), were used to describe the cell morphology.

The E was determined by the ratio between cell length and width (Kawasse et al., 2003):

$$Elongation = \frac{F_{max}}{F_{min}}$$

The F_{max} and F_{min} were determined as the maximum Feret diameter (length) and minimum Feret

diameter (width), respectively. The Feret diameter is given by the distance between two parallel tangents in any given direction.

The MN is a combination of the relevant parameters from image analysis which can be used for a holistic characterization of morphology (Wucherpfennig et al., 2011):

$$Morphology\ number = \frac{2 * \sqrt{A} * S}{\sqrt{\pi} * Fmax * E}$$

where A is the projected area (the area of the projected surface of the object on the plane of vision), S is solidity (a smooth shape has solidity of 1.0). For perfectly round and smooth pellets particles the MN has a value of one. The smallest fragment of mycelial morphology can be simplified as a one-dimensional line yielding a MN of zero. Therefore, all intermediate morphological forms will have values between 0 and 1.

CFD simulation of oil-water mixing in 1-L stirred-tank bioreactor

In order to identify the major challenges of oil mixing in bioreactors, CFD simulation by Fluent in the Ansys Workbench 17.0 was used to simulate the oil droplet dispersion in aqueous medium, which will provide clues to further optimize bioreactor design and operating conditions in real fermentation experiments with an oil substrate (Hutmacher & Singh 2008, Sarkar et al. 2016). Oil droplet size distribution and volume fraction in aqueous medium were simulated by CFD in a 2-L stirred tank (13 cm inner diameter and 24 cm height) equipped with two 6-blade Rushton turbine impellers with a 7.4-cm diameter, which are similar to the settings for Sartorius B-DCU 2-L bioreactors (Fig. 2a). During the simulation, the bioreactor's agitation speed was set at 500 rpm and the vessel was filled with water containing 5% (v/v) of corn oil. To capture the turbulent effects on the fluid flow and phase dispersion, the k-ε model was applied. The Eulerian Multiphase model in the simulations is coupled to a Discrete Population Balance Model (DPBM) to predict the size distribution of the particles and their evolution (Gelves et al., 2014; Sarkar et al., 2016).

Results

Identifying the oil-water mixing issue by CFD simulation

Mixing and mass transfer in bioreactors is known to be crucial for cell growth and production in fermentation processes. The mixing efficiency may become a limiting factor when a hydrophobic substrate such as plant oils is used as the carbon and energy source due to the insolubility of oil in water. In order to understand and analyze the major challenges of oil mixing in aqueous medium, CFD simulation for the 2-L stirred-tank bioreactor system (Sartorius B-DCU, Germany) was conducted by Fluent 17.0. The reactor vessel is equipped with two Rushton impellers running at 500 rpm, and filled with water containing 5% (v/v) of corn oil during the simulation. Figure 2a shows the bioreactor geometry along with a vertical plane for which the velocity field and oil droplet size distribution are illustrated on Fig. 2b and c. The volume fractions of oil droplet sizes of 10 μm, 200 μm, and 1000 μm are shown in Fig. 2d, e, and f, respectively.

As shown in Fig. 2c, most larger oil droplets exist in in the upper and central region of the reactor vessel. Since oil is less dense than water, the gravity force pushes oil to top regions while the centrifugation force brings oil to the center. The large droplets close the blades are broken into finer droplets and pushed into other regions of the bioreactor. In addition, smaller oil droplets (such as those with a 10-μm diameter) are much more efficiently dispersed, which leads to nearly homogenous mixing (Fig. 2d). However, the bigger oil droplets (with a diameter of around 1000 μm) are more resistant to move along with aqueous medium, thus tend to stay in upper and central regions (Fig. 2f). The simulation results suggest a significant higher agitation speed (e.g. > 1000 rpm) should be applied to break the bigger oil droplets into much smaller ones to accelerate the liquid flow and intensify the oil-water mixing in the reactor vessel. This was validated by real fermentation experiments, which is discussed in next session.

Optimization of bioreactor design and operating conditions for fermentation with oil substrates

For fermentation experiments with oil substrate, the wild type *Y. lipolytica* ATCC2032 was employed for production of CA from SbO. The 1-L bioreactor was equipped with three Rushton impellers, which has one more impeller as compared to the bioreactor geometry in CFD simulation. The third impeller was added to the top region of the bioreactor to break up the SbO into tiny and small oil droplets. There are two typical types of impellers can be used for agitation during the fermentation: the Rushton type impellers with six flat and vertical blades usually push the liquid toward the side direction and provide better flow and mixing in the radial direction; the pitched-blade impellers, however, have six blades twisted at certain angle (e.g. 45^{o}) to provide flow and mixing in both radial and axial directions, thus are able to overcome the oil droplets' buoyance forces and disperse them better in aqueous medium. For comparison in fermentation experiments, two sets of impellers were tested, with one set of impellers consisted of three evenly-spaced Rushton impellers while the other consisted of two pitched-blade impellers on top and one Rushton impeller in bottom (Fig. 3a-b). In addition, two maximum agitation speeds for the pitched-blade impellers, 1000 rpm and 1400 rpm, were tested to examine if more powerful agitation provides better mixing and improves the fermentation performance, as suggested by the previous CFD simulation results.

As shown in Fig. 3c, the DCW from the fermentation with different impellers and agitation speeds were similar, indicating that any set of the impeller and agitation conditions met with the requirements for *Y. lipolytica* cell growth on oil substrate. However, impeller type and agitation speed have significant impacts on CA production from SbO (Fig. 3d, e, and f). With 3 Rushton impellers, a CA titer of 84 g/L, a specific CA titer of 1.4 g/g DCW, and a CA conversion yield of 0.32 g/g from SbO were obtained at 144 h. By replacing the two top Rushton impellers with 2 pitched-blade ones, the CA titer, the specific CA and the CA yield increased to 95 g/L, 1.6 g/g DCW, and 0.35 g/g, respectively. This confirmed the hypothesis that the pitched-blade impellers

provide better mixing along the axial direction so that the SbO was dispersed into deeper regions of the bioreactor to be utilized by the yeast cells to convert to CA. In addition, when the maximum agitation speed decreased from 1400 rpm to 1000 rpm during the production phase, CA production titer at 144 h also decreased from 95 g/L to 68 g/L, which also validated what the CFD simulation results suggested, *i.e*. more powerful agitation could disperse the oil droplets into the regions farther from the center and form increased number of tiny droplets so that the cells were able to use them for enhanced CA production. In all further fermentation experiments that are discussed later, the 2 pitched-blade impellers and 1 Rushton impeller (Fig. 3b) with a maximal agitation speed of 1400 rpm were used.

Comparison between the fermentation experiments with glucose and oil substrates

To investigate how glucose and oil substrates affect differently on cell growth, intracellular lipid accumulation, and CA production, three sets of fed-batch fermentation with the wild type *Y. lipolytica* ATCC20362 were studied in 1-L bioreactors where glucose, SbO, and WCO were respectively supplied as the sole carbon source. The final DCW from the experiments with SbO and WCO substrate were 1.5-fold of that from the experiment with glucose (Fig. 4a). The improvements in DCW by SbO and WCO were mainly caused by increases in intracellular lipids. The final lipid/DCW from the runs with SbO and WCO were 57% and 64%, respectively, which increased by 128% and 156% as compare to the run with glucose (Fig. 4c). However, the increases in DCW and intracellular lipids by using oil substrates did not improve the further conversion to CA. The final CA titers for the runs with SbO and WCO were 70.2 g/L and 66.0 g/L, respectively, both of which were lower than the 92.3 g/L obtained from the experiment with glucose (Fig. 4b). The final conversion yields of CA from substrates were similar for all three sets of experiments, within 0.34-0.36 g/g (Fig. 4d). The lipid yields from the runs with SbO (0.15 g/g) and WCO substrate (0.16 g/g) were 4-fold higher than that from the experiment with glucose (0.03 g/g) (Fig. 4d).

Effect of cell morphology on Y. lipolytica fermentation

To investigate the effect of cell morphology on cell growth and CA production from glucose and oil substrates, strain VSYM1 was generated by expressing a second copy of *MHY1* gene in the chromosome of the wild type *Y. lipolytica* ATCC20362 while strain VSYM2 was obtained by deleting the *MHY1* gene from the chromosome. Both strains, together with ATCC20362, were further tested in both shake flask and fed-batch bioreactor experiments with either glucose or oil substrate. As shown in Fig. 5g, VSYM1 successfully demonstrated hyphal cell morphology while VSYM2 had a yeast-like (round) cell shape.

Effect of cell morphology on cell growth in shake flask experiments

In shake flask experiments with ATCC20362, VSYM1, and VSYM2, three substrates including glucose, SbO, and WCO were used and compared for cell growth. As shown in Fig. 5a, the obtained DCWs of the two engineered strains were similar to strain ATCC20362 with the same substrate, which suggests that effects of cell morphology and mixing issues may not be critical in the small-volume flask environment when cell densities are low. In addition, the final cell densities obtained from the runs using SbO and WCO were significantly higher than that from the run using glucose. This increase in cell mass should be attributed to the increase in intracellular lipid due to the use of an oil substrate. Interestingly, the run using WCO produced more biomass than the run with SbO. This should be due to more available FFAs in WCO that can be directly used by the cells.

Effect of cell morphology on cell growth and products formation in 1-L bioreactors

In 1-L fed-batch bioreactor experiments, yeast-like *Y. lipolytica* VSYM2 produced similar biomass with the wild type strain ATCC20362 for all three different substrates tested (Fig. 5b). The hyphal *Y. lipolytica* VSYM1, however, produced higher cell mass than the wild type strain

and VSYM2. The improvement in cell mass of VSYM1 over the other two strains was not due to the increase in intracellular lipid level. Instead, the intracellular lipid level of VSYM1 was much lower than the other two strains.

Intracellular lipid accumulation was significantly impacted by cell morphology. The round (yeast-like) cell shape, as exhibited by strain VSYM2, is more favorable for intracellular lipid accumulation while the hyphal morphology, as shown by VSYM1, seriously decreases the capability of intracellular lipid accumulation (Fig. 5d and f). The lipid content in biomass of VSYM1 reached only 19% for the run with glucose and 25% for the run with WCO. In addition, it was confirmed that using oil substrates (either SbO or WCO) can directly enhance the intracellular lipid level. Lipid contents up to 62% of DCW for the wild type strain ATCC20362 and 75% for VSYM2 were achieved in the experiments with WCO, while only 25% and 38% of lipids in DCW were achieved respectively when glucose was used as the substrate. The cell samples from the end of the run were stained with SBB to check the LBs formation under microscope. Fewer smaller LBs were observed in VSYM1 cells for samples from runs with all three different substrates. For strain ATCC20362 and VSYM2, more and larger LBs were observed for the samples from SbO and WCO runs than those from the glucose run (Fig. 5h), which were consistent with the lipid titer and yield analysis, as shown in Fig. 5d and f.

Similar to the impacts of cell morphology on intracellular lipids, the hyphal cell shape badly reduced the CA production (Fig. 5c). VSYM1 produced only 15~20 g/L CA while ATCC20362 and VSYM2 produced 65~100 g/L CA. The strain VSYM2 with the round cell shape only slightly improved the CA production over the wild type strain. In addition, CA conversion yields from glucose, SbO, and WCO were very similar, around 0.35 g/g for strain ATCC20362 and VSYM2 (Fig. 5e). However, the CA titer achieved from runs with SbO and WCO (66~77 g/L) were about 25% lower than from run with glucose (92~99 g/L), indicating that more metabolic pathway engineering work should be conducted in future to achieve significantly higher production titer and yield for biomanufacturing of any extracellular products from oils or fats.

Correlation between cell morphology and production of cell mass, lipids, and citric acid

In order to quantitatively analyze the impacts of cell morphology on cell growth and product formation of *Y. lipolytica*, two parameters, the Morphology number MN and the Elongation factor E, were introduced. As described in the section of materials and methods, MN is a number between 0 and 1. A perfect round cell has a MN of 1 while an infinitely long cell has a MN of 0. For the Elongation factor E, it is a number great than 1, with a larger E value denoting a more elongated cell shape. The values of both MN and E were obtained with the aid of microscopic image analysis.

As shown in Fig. 6, the results of the cell Morphology number MN and Elongation E were consistent with the cell shapes that were observed under the microscope. The Elongations Es were in the order of VSYM1 > ATCC20362 > VSYM2 (Fig. 6a, c, e) while MNs were VSYM1 < ATCC20362 < VSYM2 (Fig. 6b, d, f). More than 60% of cells in VSYM1 had Elongations Es great than 3, which were 3-fold higher than those of the wild type yeast ATCC20362. The cells of VSYM2, with round or yeast-like cell shapes, had E factors less than 1.5 were more than 70% which increased 4-fold compared to ATCC20362. The results were also consistent with distribution of the Morphology numbers MNs: about 50% of the wild type *Y. lipolytica* cells had MNs within 0.25~0.50, but 70% of VSYM1 cells had MNs less than 0.25 and 70% of VSYM2 cells had MNs greater than 0.5 (Fig. 6b, d, f).

Interestingly, a fairly good linear correlation (R^2 > 0.86) was obtained between the Elongations Es (or Morphology numbers MNs) and the obtained lipid-free dry cell weight (total DCW subtracting the total intracellular lipids) for all three *Y. lipolytica* strains (ATCC20362, VSYM1 and VSYM2) (Fig. 7a, b). Large Es or smaller MNs correlates to higher lipid-free biomass formation, which suggests the cell growth may be beneficial from the elongated cell shapes that have greater surface to attach and uptake the extracellular fatty acid substrate.

Good correlations between Es/MNs and the production of CA and intracellular lipids were

also observed ($R^2 > 0.82$) (Fig. 7c-f). Different from the effect of cell morphology on lipid-free biomass formation, the yeast-like cells seemed to be able to produce more CA and intracellular lipids. Therefore, strain VSYM2 with round shapes, which had significantly smaller Es and greater MNs, produced the most CA and intracellular lipids. The results also suggest that the product formation is more determined by the intracellular biochemical processes, and the round cell shape may be more beneficial to such biochemical processes.

Summary of oil fermentation kinetics under various bioreactor and cell morphology conditions

To quantify the effects of bioreactor design and operation condition, substrates/carbon sources, and cell morphology upon cell growth and products formation of *Y. lipolytica*, the values of major fermentation kinetic parameters, including the maximum specific growth rate μ_{max}, the biomass yield from substrate $Y_{X/S}$, the CA yield from substrate $Y_{CA/S}$, and the lipid yield from substrate $Y_{L/S}$, were compared. The μ_{max} was determined by linear regression analysis of the DCW during 0~20 h. The $Y_{X/S}$ was determined by the ratio of total production of biomass to the substrate consumed during the growth phase (0~30 h). The values of $Y_{L/S}$ and $Y_{CA/S}$ were determined by the ratio of total production of intracellular lipids and CA to the total substrate consumed in the end of each run, respectively. As shown in Table 3 (Entry 2~4), higher $Y_{X/S}$ and $Y_{CA/S}$ of ATCC20362 with the SbO substrate were obtained through increasing the maximum agitation speed and employing pitched-blades impellers, which was due to the improvement in extracellular mixing of oil droplets in aqueous medium. Under the same impellers and agitation conditions, the μ_{max} and $Y_{X/S}$ of ATCC20362 with oil substrates were slightly higher than with glucose substrate (Table 3, Entry 1 ,3, 5). The $Y_{L/S}$ significantly increased when an oil substrate was used (Table 3, Entry 3, 5). In addition, the cell morphology has slight effect on μ_{max} of *Y. lipolytica*: the hyphal shape strain VSYM1 (Table 3, Entry 6~8) had slightly lower growth rate while the yeast-like strain VSYM2 (Table 3, Entry 9~11) had slightly faster growth rate, as

compared to the wild type strain. However, more significant impacts of cell morphology on intracellular lipids and CA production were observed. The yields of CA and lipids ($Y_{CA/S}$ and $Y_{L/S}$) increased by 3-4 fold as the cell morphology changed from hypha to yeast form (Table 3, Entry 6~11).

Discussion

For fermentation products, the expense in raw materials (mainly the carbon source) contributes a significant portion of the total manufacturing cost. It is estimated that the raw materials, mainly the carbon source, may contribute to 50% or more of the total cost for biofuels and other bio-made chemicals. Therefore, reducing raw material cost is critical for economical biomanufacturing processes, which can be achieved by designing new microbial cell factories and fermentation processes that can efficiently utilize and convert the alternative raw materials other than sugars with lower cost to achieve the same or higher product yield. Over the past decade, the use of lipid substrates such as WCO for the production of practically important products by *Y. lipolytica* is becoming attractive. It was estimated that more than 10 million tons of WCOs and fats are produced each year in the U.S., and the reutilization of WCO for biomanufacturing would significantly improve its economic values and decrease the biomanufacturing cost.

Technical challenges in both extracellular oil substrate uptake and intracellular bioconversion processes need to be addressed before oils or fats become an economically viable and attractive option for large scale biomanufacturing. The strategy for overcoming the extracellular bioprocess barrier is mainly to develop a special oil/fat bioreactor system that can convert oils/fats into utilizable FFAs and provide high efficiency of mixing and mass transfer by circumventing the insolubility of oils/fats/FFAs in aqueous medium. After that, cellular and metabolic engineering strategy can be applied to convert the intracellular fatty acids into high-value products. The oleaginous yeast *Y. lipolytica*, which is able to grow directly on oils/fats, was

chosen as the host to create such a microbial cell factory for biomanufacturing from an oil substrate.

To overcome the extracellular mixing and mass transfer barrier of oils/fats in aqueous medium, we first used CFD simulation to understand and analyze the dispersion of oil droplets in aqueous medium in the stirred-tank bioreactor. The simulation results provided guidance for further experimental optimization of the impeller design and agitation speed, which eventually led to significantly higher cell growth and CA production of the wild type *Y. lipolytica* on oil substrate. Future CFD study will explore the three-phase (air-oil-aqueous medium) bioreaction system under conditions of various agitation speed, impeller types, and reactor sizes. Bioreactions with cell growth, oil uptake, and production will also be included in the CFD model. It is our expectation that the bioreactor CFD will play an extremely important role in establishing the biomanufacturing platform for high-value products from plant oils.

Another limitation step during the extracellular oil uptake process is the low lipase activity, especially after the cell growth phase. Plant oil is typically in the format of TAG, which needs to be degraded to one glycerol and three molecules of FFAs with the catalysis of lipase for further utilization. The *Y. lipolytica* yeast is able to produce lipases and release them to the medium to degrade TAG oil into FFAs, so that FFAs can be imported by the cells and further metabolized intracellularly. However, our fed-batch fermentation experiments with the wild type *Y. lipolytica* ATCC20362 showed that both oil uptake and CA production notably slow down after 48 h when the cells reached the production phase (Fig. 3d). The final CA titer was only 74% of that from the fermentation with glucose. Our further analysis of the residual FFAs and TAG oils in medium showed that the residual FFAs decreased to less than 3 g/L after 48 h though 20-30 g/L of TAG oil was remained in the medium. Therefore, the low activity of lipases in the production phase became a limited factor in TAG oil utilization and bioconversion. Previous work by Kamzolova et al. (2005) and Fickers et al. (2005b) showed that the transition of *Y. lipolytica* fermentation from the exponential growth phase to the production phase (growth retardation), which was

caused by the depletion of nitrogen in the medium, led to a decrease in specific activity of lipase. Therefore, we expect that overexpressing the lipase genes (e.g., *YlLip2*, *YlLip7* and *YlLip8*) in the *Y. lipolytica* yeast and/or adding commercially available lipases to the fermentation medium may significantly enhance the efficiency of oil uptake and further bioconversion into desired products.

The extracellular oil uptake process can also be impacted by cell morphologies. The *Y. lipolytica* cells can have either the classical yeast-like (round) cell shape or hyphal (filament) morphology. In general, longer cells may provide larger surface area to attach more oil droplets than the round cells, thus uptake the oil substrate more efficiently. Two new *Y. lipolytica* strains, VSYM1 with hyphal cell morphology and VSYM2 with the yeast-like form, were generated by overexpressing and deleting the *MHY1* gene in the wild type strain, respectively. However, both shake-flask and 1-L bioreactor experiments showed that no significant difference of cell growth on oil substrate or biomass formation between the cells of VSYM1, VSYM2, and the wild type *Y. lipolytica*. Instead, strain VSYM1 produced much less CA and intracellular lipids from SbO or WCO than the wild type strain and VSYM2 (Fig. 4). In addition, it was noticed that the viscosity of the fermentation broth for the hyphal cells of VSYM1 grown on oil, which may have led to less efficient oxygen transfer and increased power input in the stirred-tank bioreactor. At the same time, the round cell shape of VSYM2 seemed more beneficial to intracellular lipid formation and the further bioconversion of intracellular FAs to the desired products. The strain VSYM2 was able to store about 20% more intracellular lipids than the wild type strain ATCC20362 and 3-fold more than the strain VSYM1, which provided a larger substrate pool for further bioconversion of the intracellular lipids into CA. Therefore, the effect of cell morphology on the biomanufacturing with an oil substrate should take both extracellular oil uptake and the intracellular bioconversion processes into account.

The intracellular biochemical process for further converting the intracellular lipids into the desired products is not a major focus in this study due to the diversity of possible products and

different metabolic engineering strategies can be applied to make each specific product. Though this study only investigated how the wild type *Y. lipolytica* and its variants grew on plant oils and produced CA from the oil substrate, we expect that those products directly derived from lipids such as omega-3 fatty acids (Xie et al., 2015; Xie et al., 2016), long-chain diacids, fatty alcohols (Wang et al., 2016), and wax esters (Xie et al., 2017) or the products indirectly derived or benefited from using the lipids such as carotenoids (Liu et al., 2020) should be produced from oil/fats with significantly higher production titer, rate, and yield, thus become the major product portfolio from this new biomanufacturing platform. For example, using oils/fats to make lipid-derived products can achieve significantly higher conversion yield than using glucose, which has to be converted to FAs at a low yield of about 25% or less (Xu et al., 2017) before the formed FAs are further converted to the target products. As shown in the fed-batch fermentation of ATCC20362, the intracellular lipid (lipid/DCW) and lipid yield increased by 140% and 400%, respectively, when SbO or WCO were used to replace glucose as the carbon source. The improvement in lipid accumulation from an oil substrate was mainly due to the higher efficiency of *ex novo* lipid formation from plant oils than the *de novo* lipid synthesis from sugars (Garay et al 2014; Liang & Jiang, 2013; Papanikolaou & Aggelis, 2009). The high levels of intracellular lipids provide sufficient pool of fatty acid source for further biosynthesis of lipid-derived and –assisted products.

Conclusions

This study addresses key technical challenges in using the waste plant oils or animal fats for biomanufacturing of value-added products by the oleaginous yeast *Y. lipolytica*. First, CFD simulation was used to identify the oil-water mixing and mass transfer challenges, which then led to improved bioreactor design and operating conditions for enhanced fermentation performance with oil substrates. Limiting factors related to oil uptake and bioconversion during the production phase were also identified. After that, we evaluated the effect of cell morphology

on oil utilization and product formation. Good correlations between the cell morphology and biomass formation, lipid accumulation, and other products formation were obtained. In addition, the fermentation kinetics of *Y. lipolytica* with glucose, SbO, and WCO under various bioreactor conditions were studied. The data obtained will help build a general model for biomanufacturing with oil substrate in future. The research results from this paper will help establish a solid foundation of the new biomanufacturing platform that converts oils or fats into a series of value-added products.

Acknowledgments

This study was supported by NSF (#1911480), UML-WPI seed grant (2019-2020), and UML new faculty start-up fund. The authors would also like to thank Dr. Carl Lawton for providing experimental facilities and technical support.

Conflict of interest

The authors have declared no conflict of interest.

References

Abghari, A., & Chen, S. (2017). Engineering *Yarrowia lipolytica* for enhanced production of lipid and citric acid. *Fermentation, 3*(3). doi:10.3390/fermentation3030034CA

Bankar, A., S. Zinjarde, A. Telmore, A. Walke and A. R. Kumar (2018). "Morphological response of *Yarrowia lipolytica* under stress of heavy metals." *Canadian Journal of Microbiology* 64(8): 559-566.

Beopoulos, A., Chardot, T., & Nicaud, J. M. (2009). *Yarrowia lipolytica*: A model and a tool to understand the mechanisms implicated in lipid accumulation. *Biochimie, 91*(6), 692-696. doi:10.1016/j.biochi.2009.02.004

Cervantes-Chavez, J. A., & Ruiz-Herrera, J. (2007). The regulatory subunit of protein kinase A promotes hyphal growth and plays an essential role in *Yarrowia lipolytica*. *FEMS Yeast Res, 7*(6), 929-940. doi:10.1111/j.1567-1364.2007.00265.x

Chen, Y., & Vaidyanathan, S. (2012). A simple, reproducible and sensitive spectrophotometric method to estimate microalgal lipids. *Anal Chim Acta, 724*, 67-72. doi:10.1016/j.aca.2012.02.049

Coelho, M. A. Z., Amaral, P. F. F., & Belo, I. (2010). *Yarrowia lipolytica* - an industrial workhorse. *AMMB Book Chapter*.

Domínguez, A., FermiNán, E., & Gaillardin, C. (2000). *Yarrowia lipolytica*: An organism amenable to genetic manipulation as a model for analyzing dimorphism in fungi. *Contrib Microbiol, 5*, 151-172. doi:10.1159/000060349

Driouch, H., Sommer, B., & Wittmann, C. (2010). Morphology engineering of *Aspergillus niger* for improved enzyme production. *Biotechnol Bioeng, 105*(6), 1058-1068. doi:10.1002/bit.22614

Du, W., Li, W., Sun, T., Chen, X., & Liu, D. (2008). Perspectives for biotechnological production of biodiesel and impacts. *Appl Microbiol Biotechnol, 79*(3), 331-337. doi:10.1007/s00253-008-1448-8

Du, X., Fang, Z., Chen, Z., Kuang, x., & Huang, Z. (2014). Rapid quantitation and dynamic accumulation analysis of neutral lipid in yeast. *Biotechnol Bulletin, 8*, 208-214.

Fickers, P., Benetti, P. H., Wache, Y., Marty, A., Mauersberger, S., Smit, M. S., & Nicaud, J. M. (2005a). Hydrophobic substrate utilisation by the yeast *Yarrowia lipolytica*, and its potential applications. *FEMS Yeast Res, 5*(6-7), 527-543. doi:10.1016/j.femsyr.2004.09.004

Fickers, P., Fudalej, F., Le Dall, M. T., Casaregola, S., Gaillardin, C., Thonart, P., & Nicaud, J. M. (2005b). Identification and characterisation of LIP7 and LIP8 genes encoding two

extracellular triacylglycerol lipases in the yeast *Yarrowia lipolytica*. *Fungal Genet Biol, 42*(3), 264-274. doi:10.1016/j.fgb.2004.12.003

Garay, L. A., Boundy-Mills, K. L., & German, J. B. (2014). Accumulation of high-value lipids in single-cell microorganisms: a mechanistic approach and future perspectives. *J Agric Food Chem, 62*(13), 2709-2727. doi:10.1021/jf4042134.

Gelves, R., Dietrich, A., & Takors, R. (2014) Modeling of gas–liquid mass transfer in a stirred tank bioreactor agitated by a Rushton turbine or a new pitched blade impeller. *Bioprocess and Biosystems Engineering*, *37(3)*, 365-375.

Hurtado, C. A., & Rachubinski, R. A. (1999). MHY1 encodes a C2H2-type zinc finger protein that promotes dimorphic transition in the yeast *Yarrowia lipolytica*. *J. bacteriol., 181*(10), 3051–3057.

Hutmacher, D. W., & Singh, H. (2008). Computational fluid dynamics for improved bioreactor design and 3D culture. *Trends Biotechnol, 26*(4), 166-172. doi:10.1016/j.tibtech.2007.11.012

Kamzolova, S., Morgunov, I., Aurich, A., Perevoznikova, O., Shishkanova, N., Stottmeister, U., & Finogenova, T. (2005). Lipase secretion and citric acid production in *Yarrowia lipolytica* yeast grown on animal and vegetable Fat. *Food Technol. Biotechnol., 1524771*, 663-612.

Kawasse, F. M., Amaral, P. F., Rocha-Leao, M. H., Amaral, A. L., Ferreira, E. C., & Coelho, M. A. (2003). Morphological analysis of *Yarrowia lipolytica* under stress conditions through image processing. *Bioprocess Biosyst Eng, 25*(6), 371-375. doi:10.1007/s00449-003-0319-z

Kohlwein, S. D. (2010). Triacylglycerol homeostasis: insights from yeast. *J Biol Chem, 285*(21), 15663-15667. doi:10.1074/jbc.R110.118356

Kohlwein, S. D., & Paltauf, F. (1983). Uptake of fatty acids by the yeasts, *Saccharomyces uvarum* and *Saccharomycopsis lipolytica*. *Biochim. Biophys. Acta, 792*, 310–317. doi:10.1016/0005-2760(84)90198-X

Lee, N., & Kronstad, J. W. (2002). ras2 Controls morphogenesis, pheromone response, and pathogenicity in the fungal pathogen *Ustilago maydis*. *Eukaryot Cell, 1*(6), 954-966. doi:10.1128/ec.1.6.954-966.2002

Liang, M. H., & Jiang, J. G. (2013). Advancing oleaginous microorganisms to produce lipid via metabolic engineering technology. *Prog Lipid Res, 52*(4), 395-408. doi:10.1016/j.plipres.2013.05.002

Liu, N., Liu, B., Wang, G., Soong, Y.-H. V., Tao, Y., Liu, W., & Xie, D. (2020). Lycopene production from glucose, fatty acid and waste cooking oil by metabolically engineered *Escherichia coli*. *Biochem. Eng. J., 155*. doi:10.1016/j.bej.2020.107488

Lucatero, S., Larralde-Corona, C. P., Corkidi, G., & Galindo, E. (2003). Oil and air dispersion in a simulated fermentation broth as a function of mycelial morphology. *Biotechnol Prog, 19*, 285-292. doi:10.1021/bp020118e

Menisher, T., Metghalchi, M., & Gutoff, E. B. (2000). Mixing studies in bioreactors. *Bioprocess Engineering, 22*(2), 115-120. doi:10.1007/s004490050020

Mlickova, K., Roux, E., Athenstaedt, K., d'Andrea, S., Daum, G., Chardot, T., & Nicaud, J. M. (2004). Lipid accumulation, lipid body formation, and acyl coenzyme A oxidases of the yeast *Yarrowia lipolytica*. *Appl Environ Microbiol, 70*(7), 3918-3924. doi:10.1128/AEM.70.7.3918-3924.2004

Morales-Vargas, A. T., Dominguez, A., & Ruiz-Herrera, J. (2012). Identification of dimorphism-involved genes of *Yarrowia lipolytica* by means of microarray analysis. *Res Microbiol, 163*(5), 378-387. doi:10.1016/j.resmic.2012.03.002

Papanikolaou, S., & Aggelis, G. (2009). Biotechnological valorization of biodiesel derived glycerol waste through production of single cell oil and citric acid by *Yarrowia lipolytica*. *Lipid Technology, 21*(4), 83-87. doi:10.1002/lite.200900017

Refaat, A. A. (2010). Different techniques for the production of biodiesel from waste vegetable oil *Int. J. Environ. Sci. Tech., 7*, 183-213. doi:doi:10.1007/BF03326130

Ruiz-Herrera, J., & Sentandreu, R. (2002). Different effectors of dimorphism in *Yarrowia lipolytica*. *Arch Microbiol, 178*(6), 477-483. doi:10.1007/s00203-002-0478-3

Sarkar, J., Shekhawat, L. K., Loomba, V., & Rathore, A. S. (2016). CFD of mixing of multi-phase flow in a bioreactor using population balance model. *Biotechnol Prog, 32*(3), 613-628. doi:10.1002/btpr.2242

Soong, Y. H. V., Liu, N., Yoon, S., Lawton, C., & Xie, D. (2019). Cellular and metabolic engineering of oleaginous yeast *Yarrowia lipolytica* for bioconversion of hydrophobic substrates into high−value products. *Engineering in Life Sciences, 19*(6), 423-443. doi:10.1002/elsc.201800147

Wang, G., Li, D., Miao, Z., Zhang, S., Liang, W., & Liu, L. (2018). Comparative transcriptome analysis reveals multiple functions for Mhy1p in lipid biosynthesis in the oleaginous yeast *Yarrowia lipolytica*. *Biochim Biophys Acta Mol Cell Biol Lipids, 1863*(1), 81-90. doi:10.1016/j.bbalip.2017.10.003

Wang, G., Xiong, X., Ghogare, R., Wang, P., Meng, Y., & Chen, S. (2016). Exploring fatty alcohol-producing capability of *Yarrowia lipolytica*. *Biotechnol Biofuels, 9*, 107. doi:10.1186/s13068-016-0512-3

Wucherpfennig, T., Hestler, T., & Krull, R. (2011). Morphology engineering--osmolality and its effect on *Aspergillus niger* morphology and productivity. *Microb Cell Fact, 10*, 58. doi:10.1186/1475-2859-10-58

Xie, D., Jackson, E. N., & Zhu, Q. (2015). Sustainable source of omega-3 eicosapentaenoic acid from metabolically engineered *Yarrowia lipolytica*: from fundamental research to commercial production. *Appl Microbiol Biotechnol, 99*(4), 1599-1610. doi:10.1007/s00253-014-6318-y

Xie, D., Miller, E., Tyreus, B., Jackson, E. N., & Zhu, Q. (2016). Sustainable Production of Omega-3 Eicosapentaenoic Acid by Fermentation of Metabolically Engineered *Yarrowia lipolytica*. In *Quality Living Through Chemurgy and Green Chemistry* (pp. 17-33).

Xie, D., Soong, Y., Liu, N., Qin, J., & Chen, S. (2017). A New Biomanufacturing Platform for Bioconversion of Plant Oils into High-Value Products. *Adv Biochem Biotehcnol, ABIO-149*. . doi:10.29011/2574-7258

Xu, J., Liu, N., Qiao, K., Vogg, S., & Stephanopoulos, G. (2017). Application of metabolic controls for the maximization of lipid production in semicontinuous fermentation. *Proc Natl Acad Sci U S A, 114*(27), E5308-E5316. doi:10.1073/pnas.1703321114

Xue, Z., Sharpe, P. L., Hong, S. P., Yadav, N. S., Xie, D., Short, D. R., . . . Zhu, Q. (2013). Production of omega-3 eicosapentaenoic acid by metabolic engineering of *Yarrowia lipolytica*. *Nat Biotechnol, 31*(8), 734-740. doi:10.1038/nbt.2622

Zeng, W., Zhang, H., Xu, S., Fang, F., & Zhou, J. (2017). Biosynthesis of keto acids by fed-batch culture of *Yarrowia lipolytica* WSH-Z06. *Bioresour Technol, 243*, 1037-1043. doi:10.1016/j.biortech.2017.07.063

Zhang, Z. Y., Jin, B., & Kelly, J. M. (2007). Effects of Cultivation Parameters on the Morphology of Rhizopus arrhizus and the Lactic Acid Production in a Bubble Column Reactor. *Engineering in Life Sciences, 7*(5), 490-496. doi:10.1002/elsc.200700002

Zhou, J., Zhou, H., Du, G., Liu, L., & Chen, J. (2010). Screening of a thiamine-auxotrophic yeast for alpha-ketoglutaric acid overproduction. *Lett Appl Microbiol, 51*(3), 264-271. doi:10.1111/j.1472-765X.2010.02889.x

Zhu, Q., & Jackson, E. N. (2015). Metabolic engineering of *Yarrowia lipolytica* for industrial applications. *Curr Opin Biotechnol, 36*, 65-72. doi:10.1016/j.copbio.2015.08.010

Table 1. Strains and plasmids used in this study.

Strain	**Genotype**	**Phenotype**	**Source**
ATCC20362	Wild-type	ura^+	ATCC
VSYU1	*URA3*Δ	ura^-	This work
VSYM1	VSYU1*, pTEF-MHY1-tCYC1-URA3*	ura^+	This work
VSYM2	VSYU1*, MHY1*Δ*::5'MHY1-URA3-3'MHY1*	ura^+	This work
Plasmid	**Characteristics**		**Source**
pMHY1	Amp^R, pUC19 derivative that expressed *MHY1* under the control of *TEF1* promoter and *CYC1* terminator and *URA3* as selection marker.		This work
pMHY1KO	Amp^R, pUC19 derivative that expressed *URA3* under the control of *URA3* promoter and terminator, which was flanked by *MHY1* promoter and terminator.		This work

Table 2. Main fatty acids present in soybean oil and waste cooking oil (canola oil).

Fatty acids	**Composition (%)**	
	Soybean oil	**Waste cooking oil**
Stearic acid (C18:0)	6.2%	4.3%
Oleic acid (C18:1)	24.1%	56.4%
Linoleic acid (C18:2)	51.9%	24.1%
Linolenic acid (C18:3)	5.3%	8.8%
Palmitic acid (C16:0)	11.8%	5.1%
Palmitoleic acid (C16:1)	0.7%	1.3%
Total	100%	100%

Table 3. Kinetic parameters of *Y. lipolytica* ATCC20362, VSYM1 and VSYM2 grown on glucose, soybean oil or waste cooking oil substrate.

No.	Strain	Substrate	Impellers	Agitation (rpm)	μ_{max} (h^{-1})	$Y_{X/S}$ (g/g)	$Y_{CA/S}$ (g/g)	$Y_{L/S}$ (g/g)
1	ATCC20362	Glucose	2 PB + 1 Rst	500-1400	0.31	0.2927	0.3536	0.03
2	ATCC20362	SbO	2 PB + 1 Rst	500-1000	0.30	0.30	0.26	-
3	ATCC20362	SbO	2 PB + 1 Rst	500-1400	0.31	0.34	0.35	0.15
4	ATCC20362	SbO	3 Rst	500-1400	0.34	0.32	0.32	-
5	ATCC20362	WCO	2 PB + 1 Rst	500-1400	0.32	0.44	0.34	0.16
6	VSYM1	Glucose	2 PB + 1 Rst	500-1400	0.30	0.25	0.05	0.02
7	VSYM1	SbO	2 PB + 1 Rst	500-1400	0.32	0.31	0.11	0.06
8	VSYM1	WCO	2 PB + 1 Rst	500-1400	0.32	0.40	0.07	0.08
9	VSYM2	Glucose	2 PB + 1 Rst	500-1400	0.32	0.31	0.36	0.03
10	VSYM2	SbO	2 PB + 1 Rst	500-1400	0.33	0.36	0.37	0.17
11	VSYM2	WCO	2 PB + 1 Rst	500-1400	0.36	0.42	0.35	0.18

Abbreviations and Symbols: **PB**, Pitched-Blade (45º) impellers; **Rst**, Rushton impellers; **SbO**, soybean oil; **WCO**, waste cooking oil; CA, citric acid; $Y_{CA/S}$ (g/g), CA yield from carbon source, values are presented for the end of the run (0-144 h); $Y_{L/S}$ (g/g), intracellular lipid yield from carbon source, values are presented for the end of the run (0-144 h); $Y_{X/S}$, biomass yield coefficient, calculated by fitting the equation $Y_{X/S} = \Delta X / \Delta S$ within the growth phase (0-30 h); μ_{max}, maximum specific growth rate, calculated by fitting $\ln\left(\frac{X}{X_0}\right) = \mu_{max} t$ within the early growth phase (0-20 h). The results are average of two duplicate experiments.

Figure 1. An overview of metabolic engineering of *Y. lipolytica* for biomanufacturing of citric acid, wax esters, long-chain diacids, carotenoids, and omega-3 fatty acids. Abbreviations: GLUT2, glucose transporter; HK, hexokinase; PEP, phosphoenolpyruvate; α-KG, alpha-ketoglutarate; OAA, oxaloacetate; GUT1, glycerol-kinase 1; TCA cycle, tricarboxylic acid cycle; ME, malic enzyme; TAG, triacylglycerol; TGLs, TAG lipases; PYC, pyruvate carboxylase; ACC1, malonyl-CoA by carboxylase; ACL, ATP-citric acid lyase; GPD1, glycerol-3-phosphate dehydrogenase; FAA1, fatty acyl-CoA synthetase; ACS1, cytosolic acyl-CoA synthase; THIOs, Acyl-CoA thioesterases; FAS, fatty acid synthesis. Red frame: Fatty acid catabolism in β-oxidation pathway in peroxisome. Abbreviations: Pox1 to Pox6, acyl-CoA oxidases 1–6, respectively; MFE1, peroxisomal multi-functional enzyme; Pex3 and Pex10, peroxisome biogenesis factor 3 and 10, respectively. Gray box: Metabolic engineering pathway of wax esters. Abbreviations: FAR, fatty acyl CoA reductase; WS, wax ester synthase. Blue box: Pentose phosphate pathway. Abbreviations: G6PD, Glucose-6-phosphate dehydrogenase; 6PGD, 6-Phosphogluconate dehydrogenase; 6PGL, 6-Phosphogluconolactonase; G3P, glyceraldehyde3-phosphate. Purple oval: ω-oxidation pathway. Abbreviations: CYP450, cytochromes P450 enzyme; ADH, fatty-alcohol dehydrogenase; FAO, fatty alcohol oxidase; FALDH, fatty aldehyde dehydrogenase; LCDAs, long-chain diacids. White and yellow box within purple frame: Metabolic engineering of aerobic pathways for omega-3 fatty acids biosynthesis in endoplasmic reticulum. Abbreviations: C14/16E, C16/18E, C20/22E, and Δ9E are C14/C16, C16/C18, C20/C22 and Δ-9 elongases, respectively. Δ4D, Δ5D, Δ8D, Δ9D, Δ12D, Δ15D and Δ17D are Δ-4, Δ-5, Δ-8, Δ-9, Δ-12, Δ-15 and Δ-17 desaturases, respectively. Yellow box: Part of the cytosolic fatty acid synthesis pathway. Abbreviations: LPA, lysophosphatidic acid; PA, phosphatidic acid; DAG, diacylglycerol; DGA1 and DGA2 acyltransferase; PDAT, DAG acyltransferase; PL, phospholipid. Orange box: Metabolic engineering of carotenoids biosynthesis pathway. Abbreviations: DMAPP, dimethylallyl diphosphate; IPP, isopentenyl diphosphate; GPP, geranyl pyrophosphate; FPP, farnesyl pyrophosphate; GGPP, geranylgeranyl pyrophosphate; CrtE synthase; CrtB, phytoene synthase; CrtY, lycopene cyclase; Blue ovals: transporters. Dash lines: Putative route, not confirmed.

Figure 2. CFD simulation of oil-water mixing in a 2-L stirred-tank bioreactor equiped with two Rushton impellers running at 500 rpm. The total volume fraction of oil in water is 5%. (a) bioreactor geometry, (b) velocity field, (c) lipid droplet size dietribution, (d) volume fraction of 10-μm lipid droplets, (e) volume fraction of 200-μm lipid droplets, and (f) volume fraction of 1000-μm lipid droplets.

Figure 3. Fed-batch fermentation of *Y. lipolytica* ATCC20362 with soybean oil substrate in bioreactors equipped with different impellers and under different maximal agitation speed. (a-b)

Impellers design and maximal agitation speed, (c) dry cells weight (DCW), (d) citric acid titer, (e) specific citric acid, (f) citric acid yield.

Figure 4. Fed-batch fermentation results of *Y. lipolytica* ATCC20362 with glucose, soybean oil (SbO), or waste cooking oil (WCO). (a) Dry cells weight (DCW), (b) citric acid titer, (c) lipid/DCW, (d) yield of citric acid and lipid after 144 h cultivation.

Figure 5. Shake flask and 1-L bioreactor culture of ATCC20362, VSYM1 and VSYM2 with glucose, soybean oil (SbO), or waste cooking oil (WCO). (a) Dry cell weight (DCW) after 72 h cultivation in shake flask; (b) dry cells weight, (c) citric acid , (d) lipid/DCW, (e) citric acid yield and (f) lipid yield after 144 h cultivation in 1-L bioreactors; (g) cell morphology with a magnification of 1000x after 72 h cultivation in shake flask; (h) intracellular lipid bodies stained by Sudan black B (arrow) after 144 h cultivation in 1-L bioreactors.

Figure 6. Elongation factor (E) and Morphology number (MN) distribution for *Y. lipolytica* in bioreactors with glucose or waste cooking oil substrate after 144 h of cultivation. (a-b) ATCC20362, (c-d) VSYM1 and (e-f) VSYM2. The E and MN distribution for cells with soybean oil substrate are similar to the cells with waste cooking oil substrate. The legends for (b-f) are same as (a). At least 100 cells were analyzed for each sample.

Figure 7. Correlation of cell morphology of all conducted *Y. lipolytica* (ATCC20362, VSYM1 and VSYM2) cultivations with lipid free biomass, citric acid and lipid production. Lipid free dry cells weight over Elongation (a) and Morphology number (b); specific citric acid over Elongation (e) and Morphology number (f); lipid/DCW over Elongation (e) and Morphology number (f). The correlation and R^2 are shown in the graph. Each dot represents a single 1-L cultivation. The legends for (b-f) are same as (a). DCW: dry cells weight.

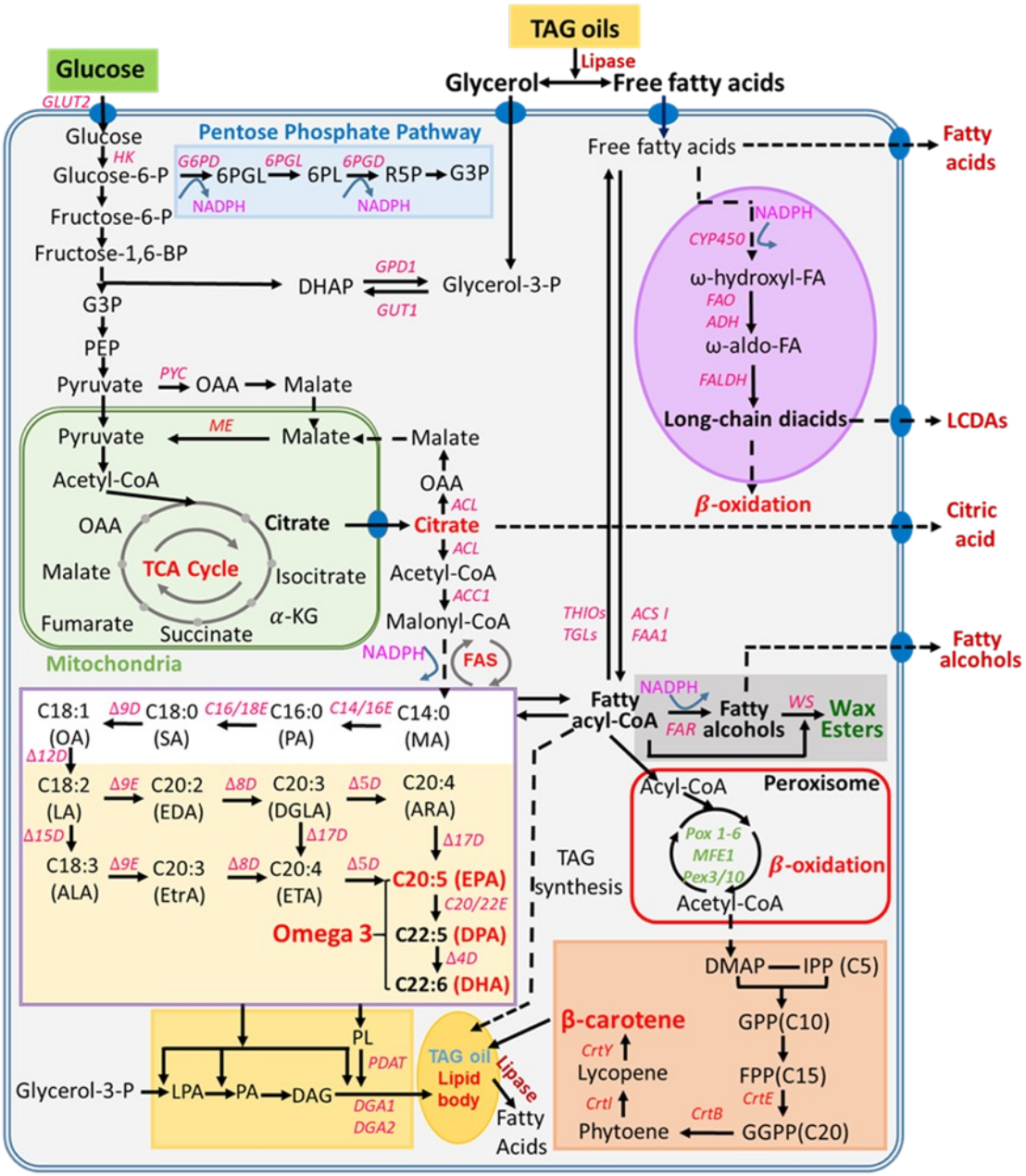
TAG oils
Lipase
Glycerol
Free fatty acids
Glucose
GLUT2
Glucose
HK
Glucose-6-P
Pentose Phosphate Pathway
G6PD
6PGL
6PGD
6PL
R5P
G3P
NADPH
NADPH
Fructose-6-P
Fructose-1,6-BP
DHAP
GPD1
GUT1
Glycerol-3-P
G3P
PEP
Pyruvate
PYC
OAA
Malate
Free fatty acids
Fatty acids
NADPH
CYP450
ω-hydroxyl-FA
FAO
ADH
ω-aldo-FA
FALDH
Long-chain diacids
LCDAs
β-oxidation
Citric acid
Pyruvate
ME
Malate
Malate
Acetyl-CoA
OAA
ACL
Citrate
OAA
Citrate
Malate
TCA Cycle
Isocitrate
ACL
Acetyl-CoA
Fumarate
α-KG
Succinate
ACC1
Malonyl-CoA
Mitochondria
NADPH
FAS
THIOs
TGLs
ACS I
FAA1
Fatty alcohols
C18:1 (OA)
Δ9D
C18:0 (SA)
C16/18E
C16:0 (PA)
C14/16E
C14:0 (MA)
Fatty acyl-CoA
NADPH
FAR
Fatty alcohols
WS
Wax Esters
Δ12D
C18:2 (LA)
Δ9E
C20:2 (EDA)
Δ8D
C20:3 (DGLA)
Δ5D
C20:4 (ARA)
Acyl-CoA
Peroxisome
Δ15D
Δ17D
Δ17D
C18:3 (ALA)
Δ9E
C20:3 (EtrA)
Δ8D
C20:4 (ETA)
Δ5D
C20:5 (EPA)
Pox 1-6
MFE1
Pex3/10
β-oxidation
TAG synthesis
C20/22E
Omega 3
C22:5 (DPA)
Acetyl-CoA
Δ4D
C22:6 (DHA)
DMAP
IPP (C5)
β-carotene
GPP(C10)
PL
PDAT
TAG oil
Lipase
CrtY
Lycopene
FPP(C15)
Glycerol-3-P
LPA
PA
DAG
Lipid body
Crtl
CrtE
CrtB
Fatty Acids
Phytoene
GGPP(C20)
DGA1
DGA2

Figure 1

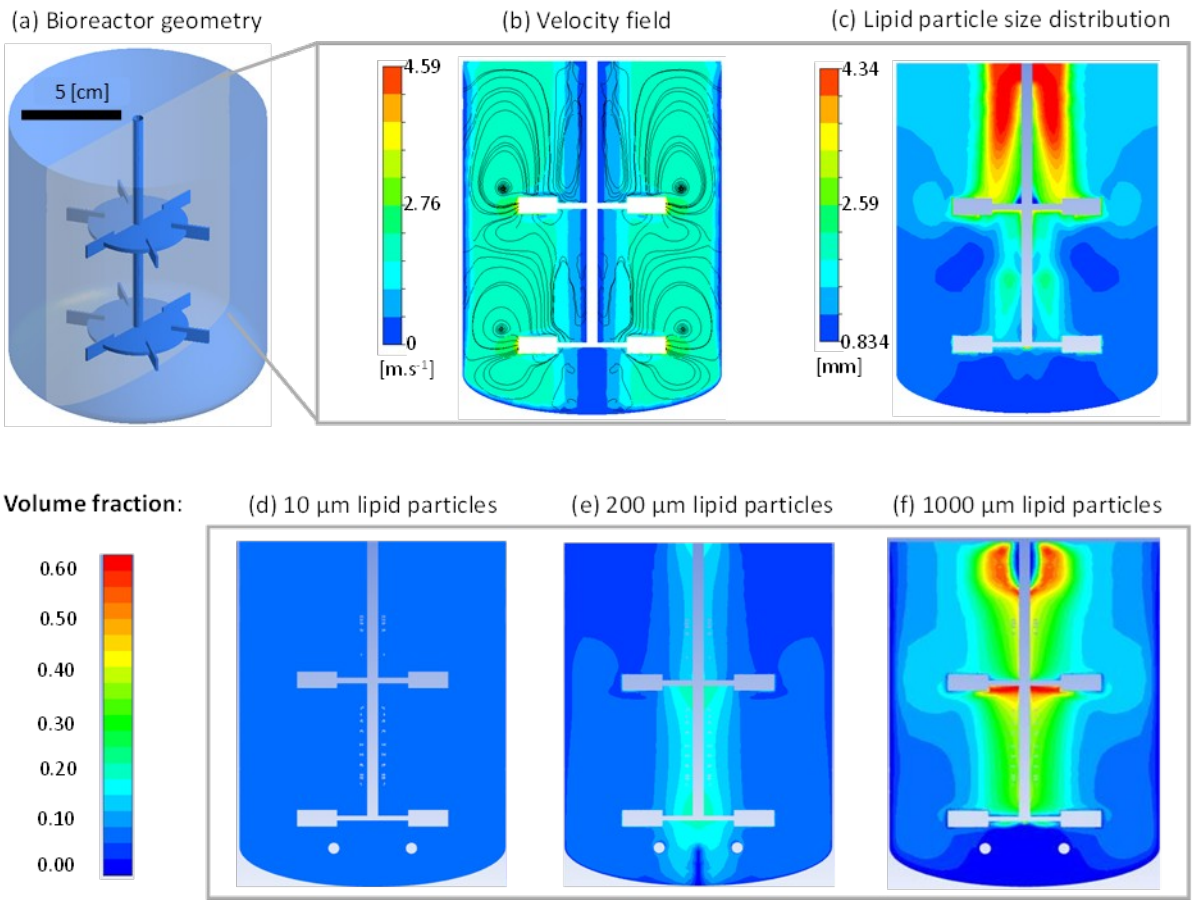
(a) Bioreactor geometry
5 [cm]
(b) Velocity field
4.59
2.76
0
[m.s-1]
(c) Lipid particle size distribution
4.34
2.59
0.834
[mm]
Volume fraction:
0.60
0.50
0.40
0.30
0.20
0.10
0.00
(d) 10 µm lipid particles
(e) 200 µm lipid particles
(f) 1000 µm lipid particles

Figure 2

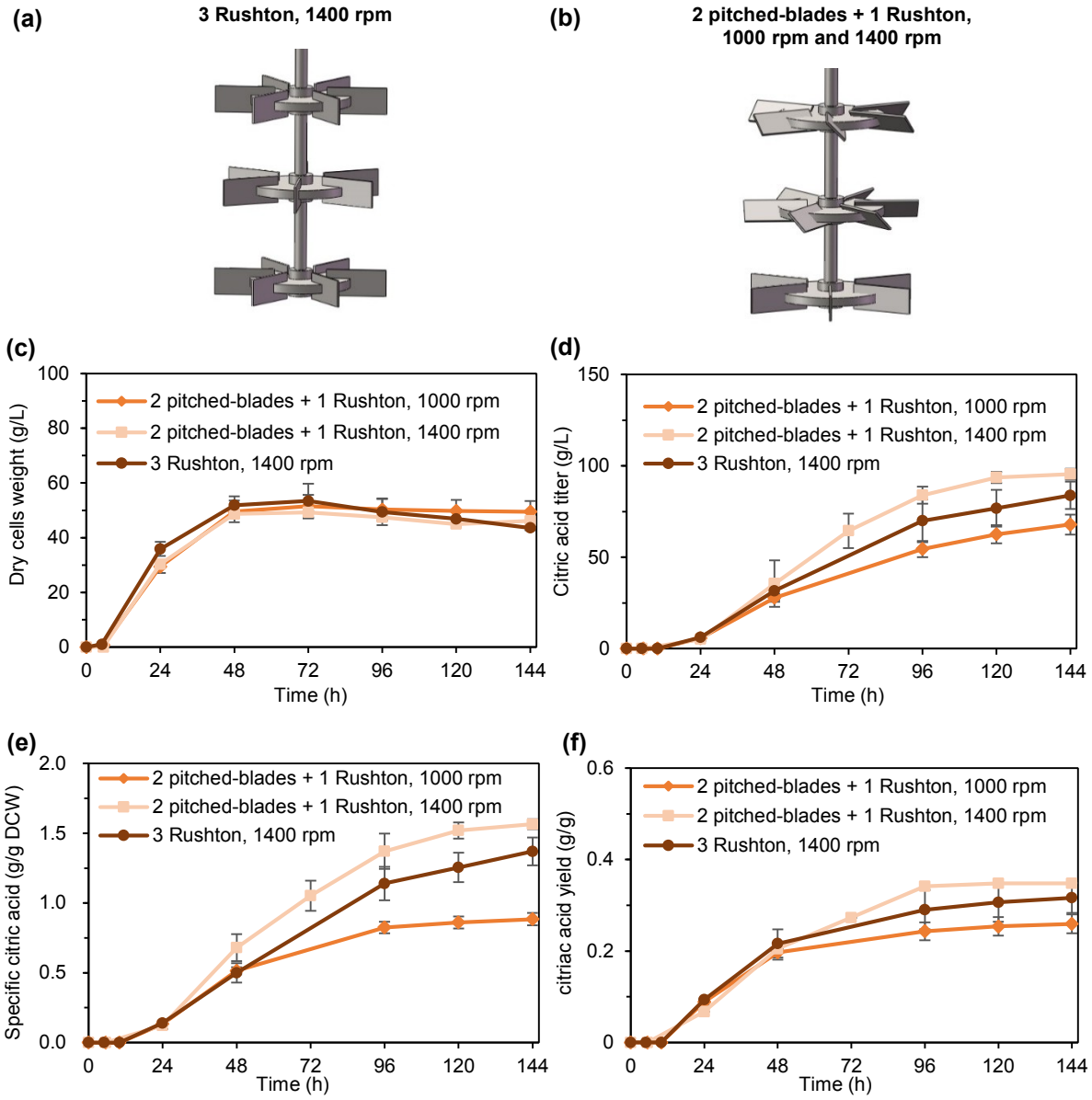
(a)
3 Rushton, 1400 rpm
(b)
2 pitched-blades + 1 Rushton, 1000 rpm and 1400 rpm
(c)
Dry cells weight (g/L)
Time (h)
2 pitched-blades + 1 Rushton, 1000 rpm
2 pitched-blades + 1 Rushton, 1400 rpm
3 Rushton, 1400 rpm
(d)
Citric acid titer (g/L)
Time (h)
(e)
Specific citric acid (g/g DCW)
Time (h)
(f)
citriac acid yield (g/g)
Time (h)

Figure 3

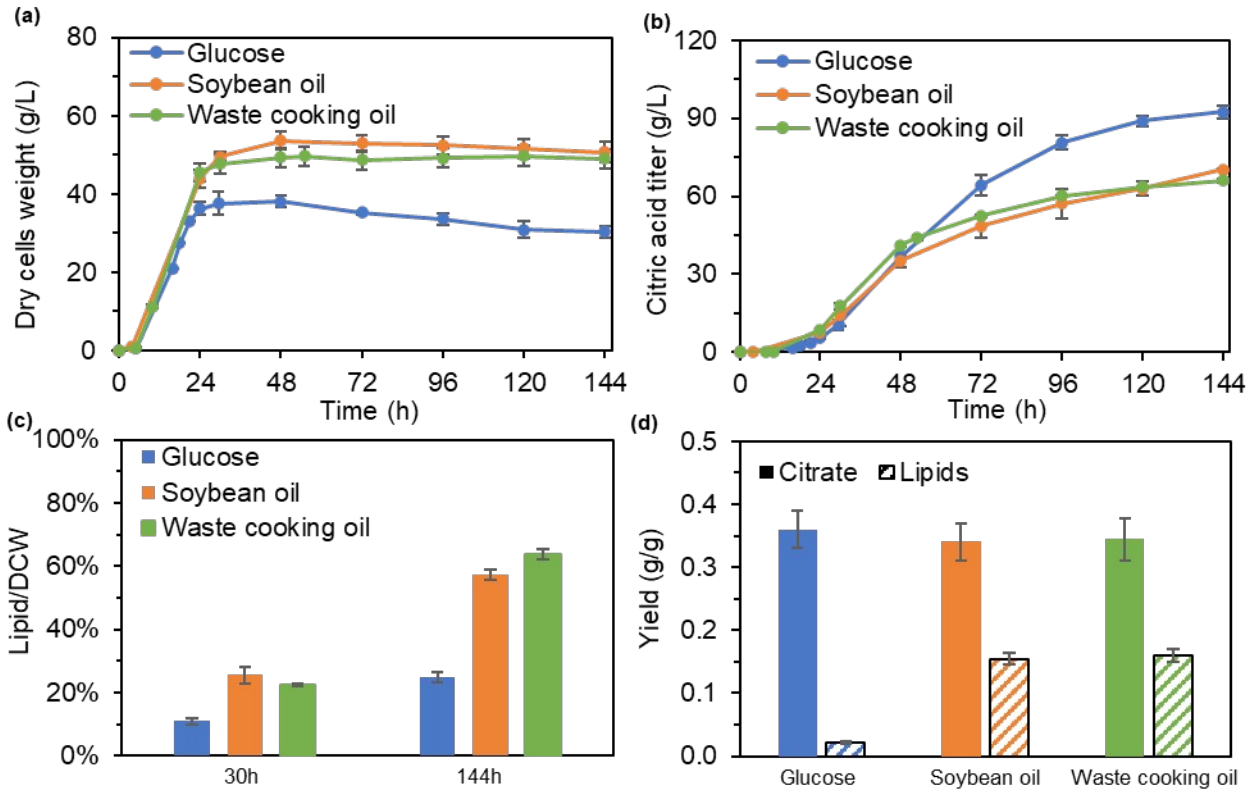
(a)
Dry cells weight (g/L)
Glucose
Soybean oil
Waste cooking oil
Time (h)
(b)
Citric acid titer (g/L)
Glucose
Soybean oil
Waste cooking oil
Time (h)
(c)
Lipid/DCW
Glucose
Soybean oil
Waste cooking oil
30h
144h
(d)
Yield (g/g)
Citrate
Lipids
Glucose
Soybean oil
Waste cooking oil

Figure 4

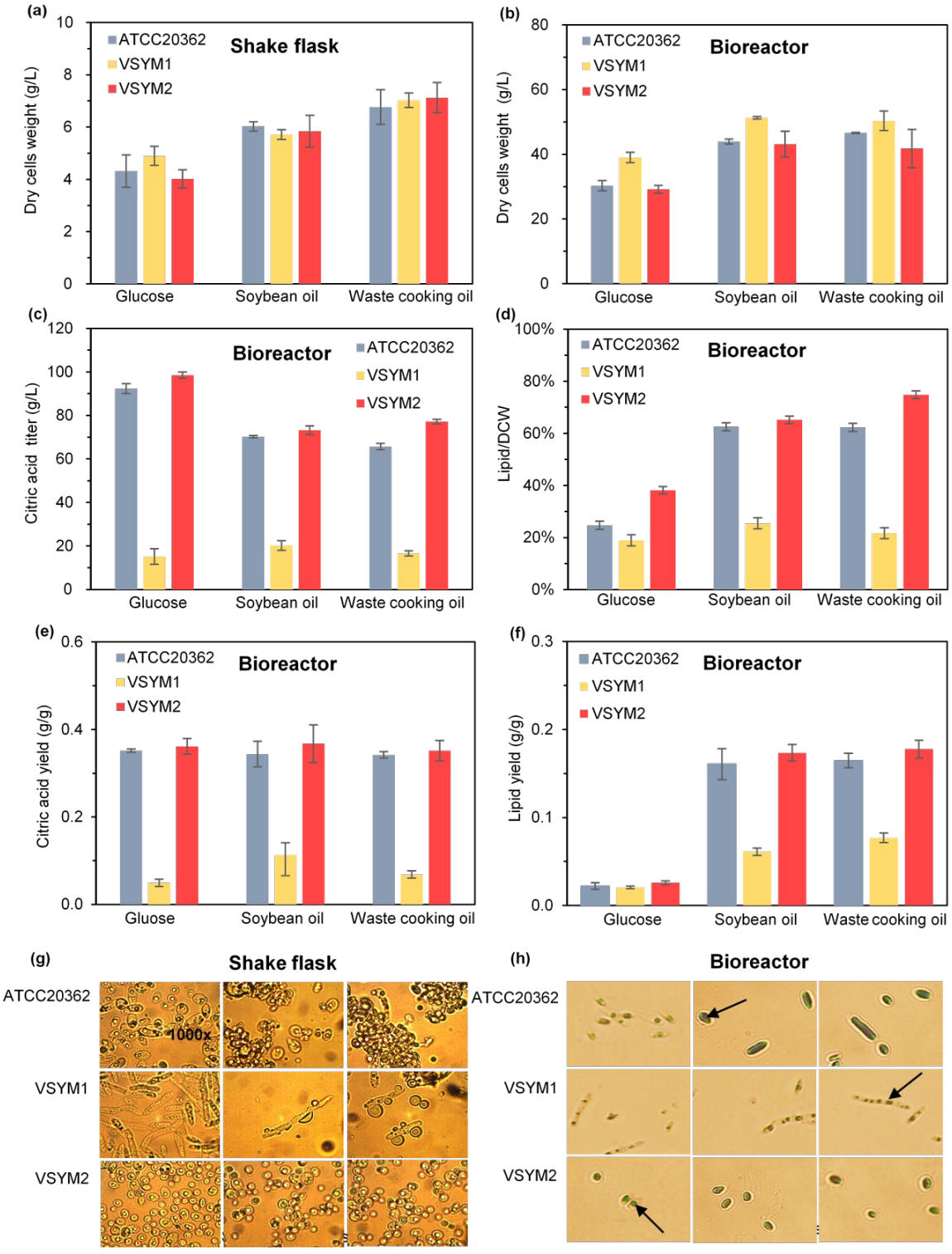
(a)
Shake flask
ATCC20362
VSYM1
VSYM2
Dry cells weight (g/L)
Glucose
Soybean oil
Waste cooking oil
(b)
Bioreactor
(c)
Citric acid titer (g/L)
(d)
Lipid/DCW
(e)
Citric acid yield (g/g)
Gluose
(f)
Lipid yield (g/g)
(g)
1000x
(h)

Figure 5

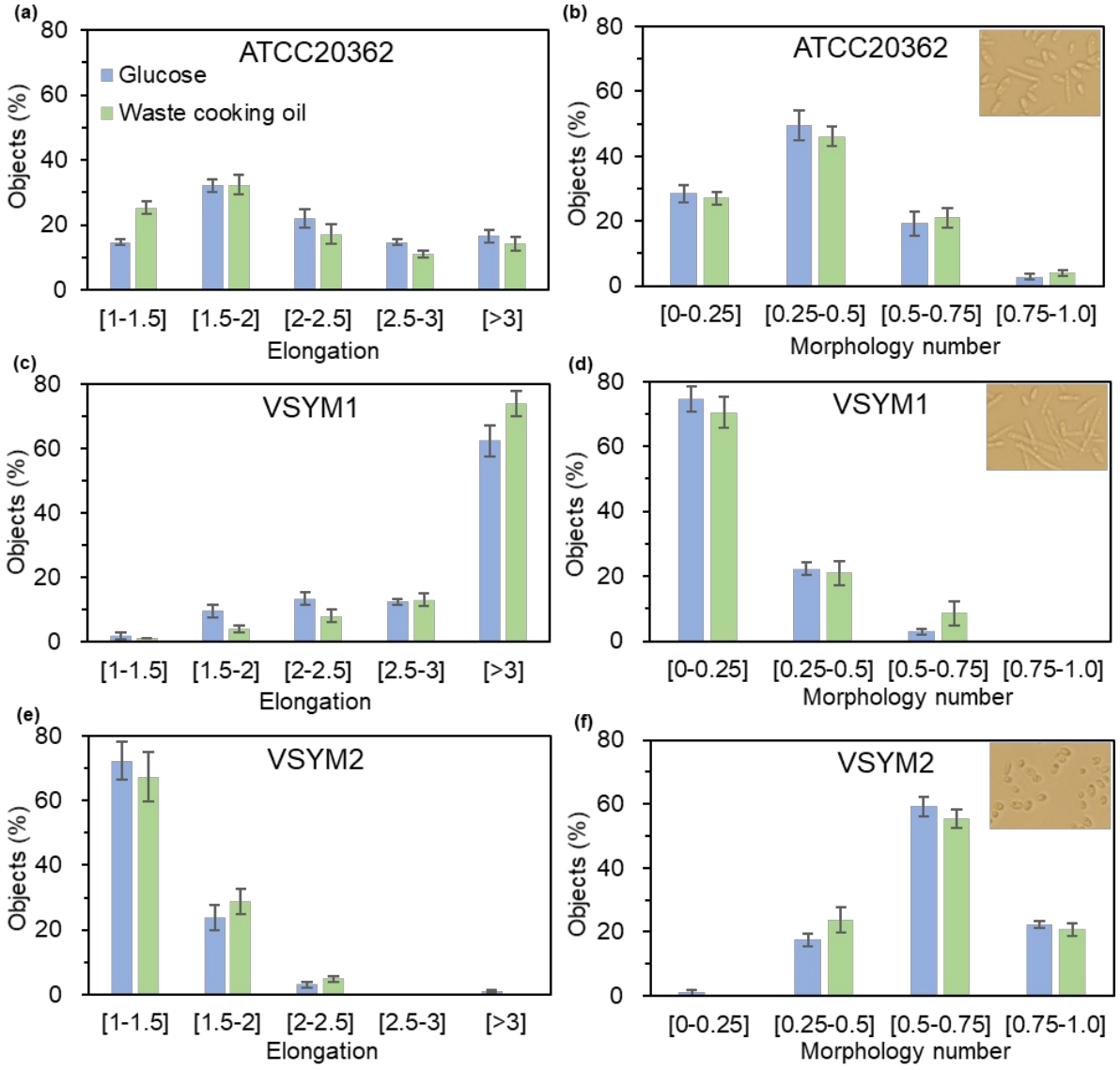
(a)
ATCC20362
Glucose
Waste cooking oil
Objects (%)
Elongation
[1-1.5]
[1.5-2]
[2-2.5]
[2.5-3]
[>3]
(b)
ATCC20362
Morphology number
[0-0.25]
[0.25-0.5]
[0.5-0.75]
[0.75-1.0]
(c)
VSYM1
(d)
VSYM1
(e)
VSYM2
(f)
VSYM2

Figure 6

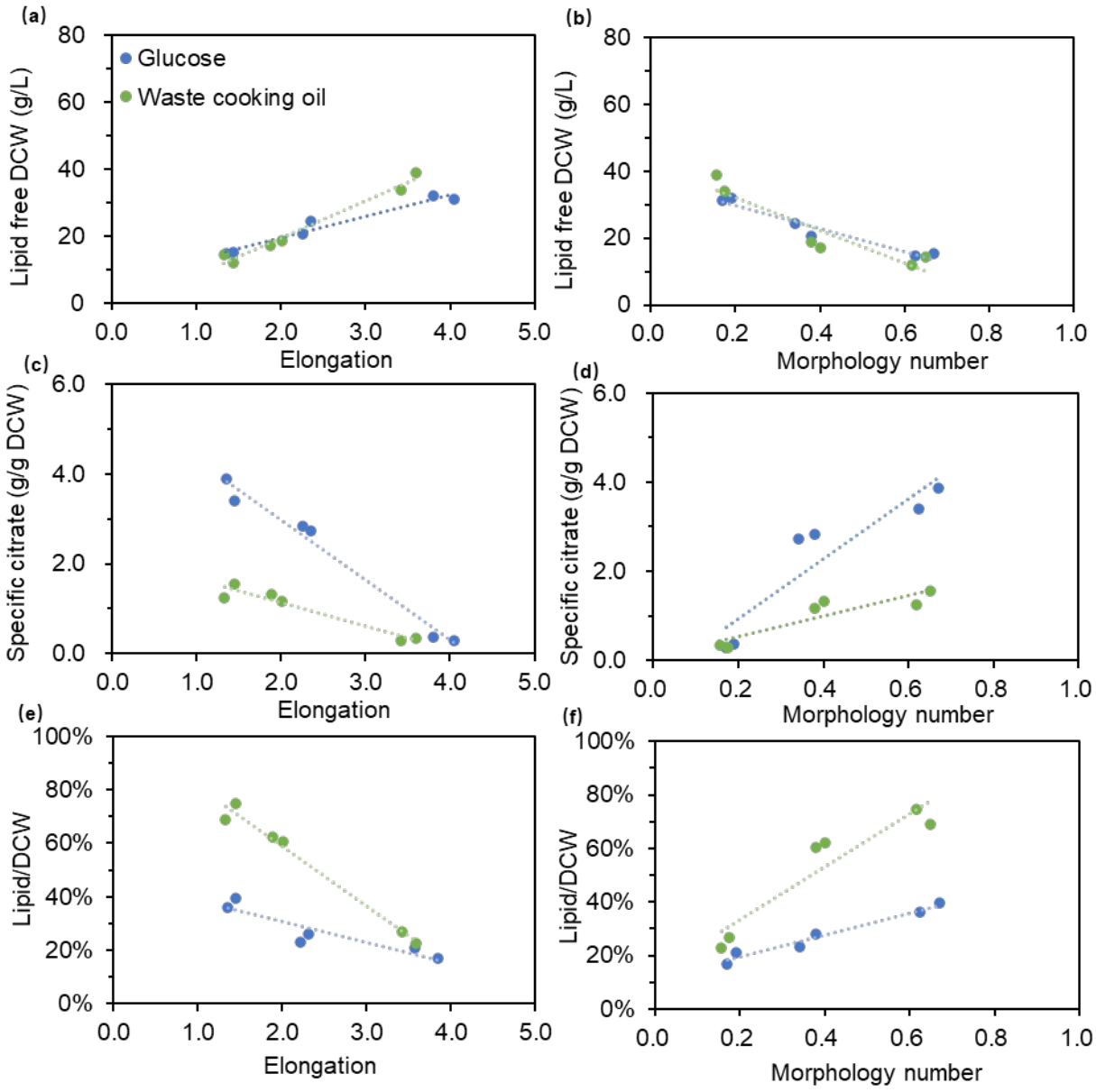
(a)
Glucose
Waste cooking oil
Lipid free DCW (g/L)
Elongation
(b)
Lipid free DCW (g/L)
Morphology number
(c)
Specific citrate (g/g DCW)
Elongation
(d)
Specific citrate (g/g DCW)
Morphology number
(e)
Lipid/DCW
Elongation
(f)
Lipid/DCW
Morphology number

Figure 7